Time-domain Line-shape Analysis from 2D Spectroscopy to Precisely Determine Hamiltonian Parameters for a Photosynthetic Complex

Brian S. Rolczynski,[1] Shu-Hao Yeh,[1,2] Polina Navotnaya,[1] Lawson T. Lloyd,[1] Alan R. Ginzburg,[1] Haibin Zheng,[1] Marco A. Allodi,[1] John P. Otto,[1] Khuram Ashraf,[3,†] Alastair T. Gardiner,[3,#] Richard J. Cogdell,[3] Sabre Kais,[4] and Gregory S. Engel[1,*]

[1]*Department of Chemistry, The Institute for Biophysical Dynamics, and The James Franck Institute, The University of Chicago, Chicago, Illinois 60637, USA*

[2]*Qatar Environment and Energy Research Institute, Hamad Bin Khalifa University, Qatar Foundation, Doha, Qatar*

[3]*Institute of Biomedical and Life Sciences, Glasgow Biomedical Research Centre, University of Glasgow, Glasgow G12 8QQ, Scotland, United Kingdom*

[4]*Department of Chemistry, Purdue University, West Lafayette, Indiana, USA*

† Current affiliation: Department of Biochemistry, Physiology and Molecular Biophysics, Columbia University, New York, New York 10027

Current affiliation: Laboratory of Anoxygenic Phototrophs, Centre ALGATECH, Novohradska 237, 379 01 Třeboň, Czech Republic

* Corresponding author, email: gsengel@uchicago.edu

Abstract

Optical signals come from coherences between quantum states, with spectral line widths determined by the coherences' dephasing dynamics. Using a 2D electronic spectrometer, we observe weak coherence-time-domain signals persisting to 1 ps in the Fenna-Matthews-Olson complex at 77K. These are coherences between the ground and excited states prepared after the complex interacts once or three times with light, rather than zero-quantum coherences that are more frequently investigated following two interactions. Here, we use these small but persistent signal components to isolate spectral contributions with narrowed peaks, and reveal the system's eigenenergies.

Introduction

Optical spectroscopy can probe the energy levels and dynamics of chemical systems but, in complex systems, spectral broadening often complicates the analysis of the underlying electronic structure. Photosynthetic pigment-protein complexes are often challenging in this regard because they involve many identical, electronically coupled chromophores to perform electronic energy transport, yielding many optical transitions at similar frequencies. Despite the broadening, to understand the processes and dynamics in systems like these, it is important to understand the energies of the individual electronic states.

For instance, the energy levels have been pursued in the Fenna-Matthews-Olson complex (FMO). Like other pigment-protein complexes, FMO has attracted attention for its efficient energy transport, which is likely due to the proteins' abilities to control the alignment of their energy levels, coupling, and embedded chromophores' positions. FMO also has other

convenient properties that contributed to its study, such as a linear absorption spectrum that overlaps well with the spectrum of a Ti:Sapphire light source, its history as the first photosynthetic protein to have a published X-ray structure,[1] and its relatively simple structure for a pigment-protein complex. Its coherent quantum dynamics have been studied since 1998[2-3] and, over that time, earlier interpretations have been supplanted by others that question the biological relevance.[4] However, the question of FMO's energy structure predates studies of its coherent dynamics, as knowledge of the energy structure is important to understand both its incoherent and coherent dynamics. The purpose of this study is to determine the energy levels of FMO's eigenstates.

FMO's Q_y band contains eight electronic energy levels in an 800 cm^{-1} window, and understanding the corresponding peak positions is important for simulating or understanding the dynamics of this system. In the last three decades, both the proposed exciton energies and the tools used to deduce them have advanced. In 1992, Pearlstein et al. applied a fit to the linear absorption spectrum of FMO to obtain peak positions.[5] Later studies in that decade considered additional evidence such as linear dichroism,[6] circular dichroism,[7] and transient absorption spectra.[8] More recent studies employed 2D spectroscopy, genetic algorithms, and quantum mechanical models.[9-13] In 2009, an eighth bacteriochlorophyll site was reported in FMO, causing renewed investigation of the electronic energies because previous investigations had assumed that only seven peaks composed the spectrum.[14] Subsequently, the energy level and dynamics of the eighth exciton were studied using a combination of experimental and theoretical techniques.[15-17] Mutagenesis was used to knock out individual sites, and the resulting linear absorption and circular dichroism spectra were measured.[18] While this method was revealing, mutations

can also have side effects on neighboring sites and their vibrational couplings.[19] Milder and coworkers have provided a review of many of these studies.[20] While this sustained effort has made substantial progress in deducing the eigenenergies, it would be beneficial to observe the peak positions directly.

When excited optically, coupled chromophores emit a signal according to their excitonic transition energies and oscillator strengths. Rapid fluctuations of the energy levels over time can result in decoherence.[21] Stochastic, multimode, Brownian oscillator models provide analytical descriptions for these processes.[22] These models describe exponential or Gaussian time-domain decay functions in the homogeneous or inhomogeneous broadening limits, respectively, and provide useful rules of thumb for the spectral characteristics in these limits.

Here, we take advantage of these dynamics to identify peak positions within the spectra. We acquire 2D electronic spectra of the Fenna-Matthews-Olson complex using a previously described non-collinear 2D spectrometer.[23] In this spectroscopic method, the sample interacts with light four times, and the signal is measured as a function of the time delays between each of these interactions. These are known as the coherence-, waiting-, and rephasing-time domains, respectively. When the coherence- and rephasing-time domains are converted to their respective frequency domains by Fourier transform, 2D spectra are obtained as a function of the waiting time, which is analogous to the time delay in a transient absorption experiment.

The coherence- and rephasing-time domain dynamics discussed here are different from the waiting-time dynamics that have often been debated previously.[4, 24] Whereas these discussions often involve signals that beat with respect to waiting time, due to zero-

quantum coherences within that time domain, the signals we discuss here are one-quantum coherences in the coherence- and rephasing-time domains. Questions about the signal attribution in the waiting-time domain arise, in large part, because of the many possible electronic and vibrational configurations a system (initially in its ground state) can access after two interactions with light. The possibilities include vibrational wavepackets within a single ground or excited electronic state, electronic coherences between distinct excited states, and more variations such as vibrons that involve mixed electronic and vibrational states.[9, 25-26] In FMO, the spacing between vibrational modes, and those between the excited electronic states, are similar in energy, so the assignment of particular beating signals to coherences between vibrational, electronic, or vibronic states requires care and has elicited debate. However, this issue is particular to the ambiguous contributions of the electronic and vibrational states to the zero-quantum signal patterns, which only appear in the waiting-time dynamics. In contrast, neither the coherence- nor rephasing-time domains feature zero-quantum coherences.

This study seeks the Hamiltonian's eigenvalues regardless of which physical states (electronic, vibrational, or vibronic) compose them. Its approach is to use a method that selectively filters the signal components producing the most spectral broadening, in order to deduce the peak positions of otherwise highly overlapping peaks within the spectra. Using 2D spectroscopy at 77 K, weak but persistent signals remain 1 ps after excitation from the coherences between the ground and excited states. Due to the low temperature and the low intensity of these signals, their existence at 1 ps does not address discussions of functionally or biologically relevant dynamics, but this study will demonstrate that the signals can nonetheless be used to distinguish overlapping spectral features in the optical

spectra. A time-domain filtering method[27] is used to isolate narrowed spectral peak contributions in experimentally measured spectra, and determine the eigenenergies of the system by direct observation. This method is first tested on calculated spectra obtained using the hierarchical equations of motions (HEOM),[28] which produces accurate spectral line shapes within the Drude approximation applied here.

Methods

Sample preparation. FMO was extracted from *C. tepidum*, as described previously.[29] It was prepared at pH = 8.0 in a 800 mM tris-HCl buffer with 50 mM NaCl and 0.1% lauryldimethylaminoxide, and prepared in a 65:35 glycerol:buffer ratio. Subsequently, it was loaded into a cuvette treated with Sigmacote (Sigma Aldrich), with a path length of 200 μm. The sample was vitrified and held at 77 K using a liquid nitrogen cryostat.

Two-dimensional electronic spectroscopy. Using a spectrometer that was described previously,[23] two-dimensional spectra were acquired from the FMO sample at 77 K. In this technique, four beams are incident on the sample in a boxcar geometry, with controlled time-delays, resulting in a signal from the sample. Beams 1-3 interact with the sample once each, while the fourth beam is highly attenuated and acts as a local oscillator.[30] The time-delays between the 1-2, 2-3, and 3-signal pulse pairs are the coherence (τ), waiting (T), and rephasing (t) times, respectively. For further information about the experimental design, see Sec. 1 of the SI. The coherence time spanned -1001 to 2002 fs in 3.5 fs steps, while the waiting time spanned 0 to 1860 fs in 30 fs steps. The step size in coherence time induces aliasing. Nonetheless, it was selected in order to make the scan feasible using the picoseconds-long range in both the coherence- and waiting-time domains. Using the current parameters, each complete set of 2D spectra took approximately 24 hours to measure. Prolonging a single

experiment much longer than that risks laser instability, cryostat failures, sample degradation, and other faults. For further discussion of the aliasing, see Section 7 in the SI.

The rephasing and non-rephasing components of the signal are measured at the positive and negative regions of τ, respectively. Data along the rephasing-wavelength domain were measured by spectral interferometry of the signal and local oscillator pulses.[30] The pulses were compressed to 14 fs (fwhm), with a repetition rate of 5 kHz and a fluence of 640 pW/μm^2 within a 100 μm diameter. Scatter-subtraction was accomplished by using shutters in beams 1 and 2 together, and separately in beam 3, and using these resulting signals to perform background subtraction.[30]

Hierarchical equations of motion. The HEOM calculations were performed using previously published methods (see Sec. 1 of the SI),[16, 28, 31-32] in order to calculate the 2D spectra shown subsequently in Figure 1, as well as Figures S2 and S5 in the Supplemental Information. A weighted average is obtained of the seven- and eight-site spectra assuming a 1/3 site VIII occupancy, reflecting the fact that site VIII is not as tightly bound as the other chromophores and can be absent from some of the proteins in the ensemble.[15] This model applies a Drude spectral density model, without the addition of embedded peaks representing the influence of particular additional vibrational modes, which could increase decoherence rates. However, the signal components investigated here, which persist at 1 ps, are already recognized to be a small portion of the power spectrum, and the approach used here does not depend on their having a large intensity as long as they can be measured.

Results and Discussion

In the coherence- and rephasing-time domains, signals appear as damped, sinusoidal time series.[22] The lineshape function initially decays often within tens to a few hundred femtoseconds, with a shape that is nearly Gaussian and/or exponential; but under the experimental conditions used here, this function has a tail that persists weakly to 1 ps. By focusing on the tail of this function, the spectral line width can be narrowed. This benefit comes at the expense of the signal intensity.

The damping occurs due to interactions between the electronic system and its environment, potentially leading to multiple, distinct broadening contributions. When the environment is modeled by multiple harmonic oscillators undergoing Brownian motion, the homogeneous broadening contributions occur in the limit of strong electronic-nuclear interactions (Δ) and slow vibrational relaxation rates (Λ), while the opposite conditions produce inhomogeneous broadening contributions.[22] This model also continuously interpolates between these limits. The homogeneous and inhomogeneous contributions dominate different regions of the coherence- and rephasing-time domains. This damping is represented by the dephasing term $g(t')$ (eq. 1). After expanding in a Taylor series and applying the conditions specified above for Δ and Λ, $g(t')$ reduces to eqs. 2 and 3 in the inhomogeneous and homogeneous limits, respectively.[22]

$$g(t') = \left[\left(\frac{\Delta}{\Lambda}\right)^2 - \frac{i\lambda}{\Lambda}\right][exp(-\Lambda t') + \Lambda t' - 1] \quad (1)$$

$$g(t')_i = \frac{\Delta^2}{2} t'^2 \quad (2)$$

$$g(t')_h = \left(\frac{\Delta^2}{\Lambda} - i\lambda\right) t' \quad (3)$$

Here, λ is the electronic-nuclear coupling strength, and t' is the given time domain (τ, T, or t). In the time-domain signal, eqs. 1-3 are applied as a decaying signal envelope by

multiplication of exp $\left(-g(t')\right)$ to the undamped time-domain signal.[22] $g(t')_i$ is proportional to t'^2 and yields a Gaussian envelope in the conjugate Fourier domain, while $g(t')_h$ is proportional to t' and yields an exponential decay in it. If all else is equal, the Gaussian contribution dominates at early time delays but quickly decays, while the exponential term is persists afterward and therefore dominates at later times.

2D spectra of FMO were obtained both experimentally and computationally, as described in the Methods section. Representative experimental rephasing-time-domain data are shown using line cuts at $\omega_\tau = 12102, 12261, 12337, 12425, 12543, 12596, 12627,$ and 12712 cm^{-1} (Fig. 1). These wavenumbers subsequently will be assigned to excitons 1-8 in FMO.

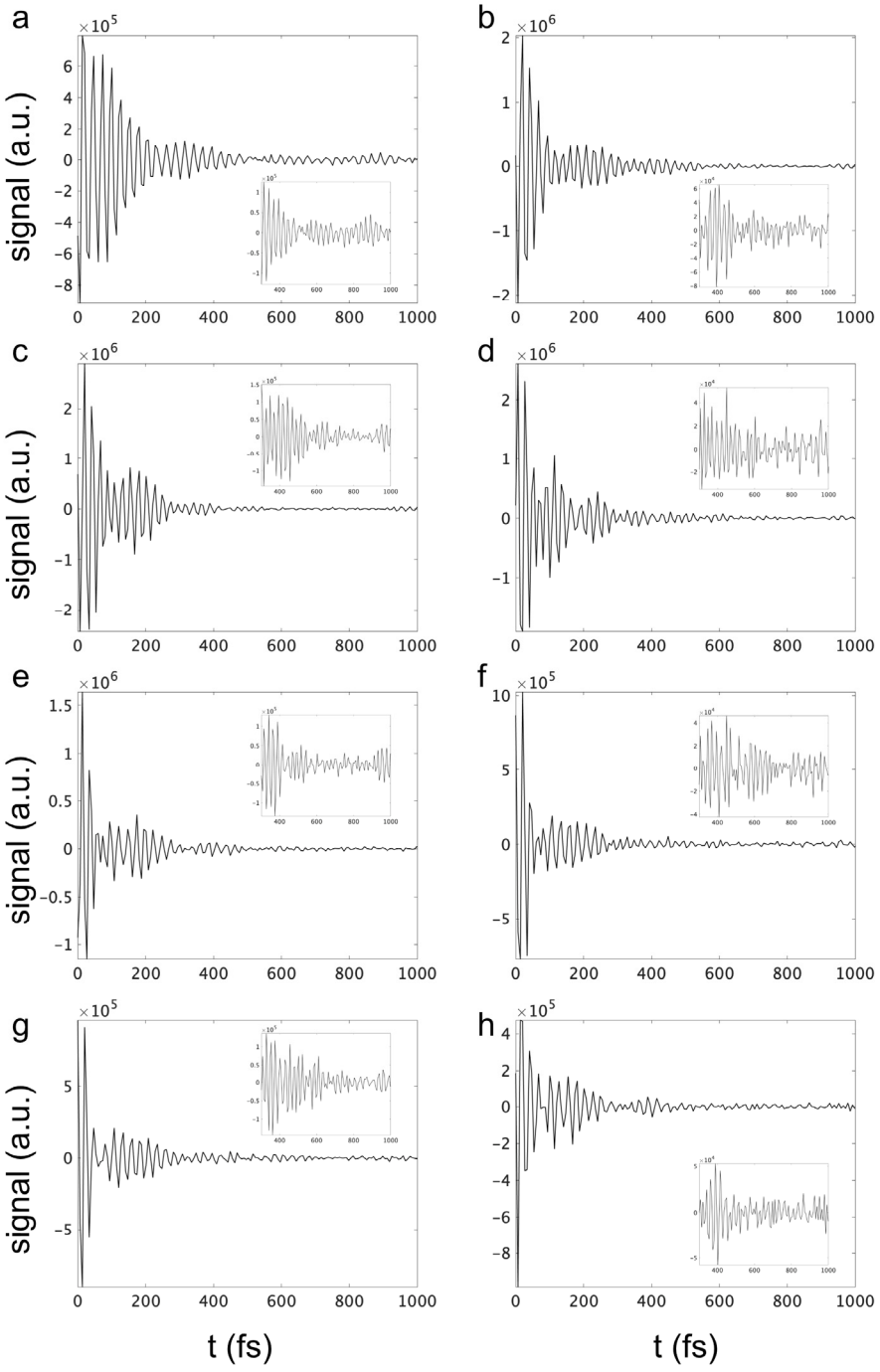

Figure 1. Measured rephasing-time-domain line-shapes are shown at ω_τ = 12102, 12261, 12337, 12425, 12543, 12596, 12627, and 12712 cm^{-1} (a-h), which subsequently will be obtained as the exciton energies in FMO. The insets focus on the range from 300-1000 fs, to show the small signals that persist in that range. For reference, corresponding measured 2D spectra are shown in Fig. 3. The signal components persisting to 1 ps are a small component of the overall power spectrum. For a discussion about aliasing in these data, see section 8 of the SI.

Weak signal components persisting at 1 ps are evident in these time series. However, the Drude oscillator model in the computed spectra may have slowed the decoherence rate, compared to spectral density models that contain particular, strongly coupled vibrational modes. Our strategy is to use the Lorentz-Gauss filter to emphasize this long-lived signal component, in order to obtain more narrow spectral peaks.

To accomplish spectral narrowing, a coherence- and rephasing-time-domain filter is applied to reduce the influence of the strongest damping contributions. This general method is discussed by Hamm and Zanni in the context of 2D infrared spectroscopy,[33] and here it is applied in 2D electronic spectra. Furthermore, coherence-time-domain data have previously been filtered in simulated 2D spectra to obtain information about the energy- or charge-transfer dynamics in diatomic or generic two-state systems,[34-35] to assign vibronic contributions in simulated spectra of FMO,[36] and to observe its electronic-environmental interactions.[37]

We use a filter similar to a Lorentz-Gauss function that was reported previously in NMR to produce narrow peak widths.[27] A Lorentz-Gauss filter $L(t')$ contains Gaussian and exponential components (eq. 4).

$$L(t') = \exp\left(\ln 2 \frac{t'-t_0'}{a}\right) \exp\left[-\frac{\ln 2}{4a}\Gamma^2(t'-t_0')^2\right] \qquad (4)$$

Here, t_0' is the lag time, Γ is a line-width reduction ratio, and a corresponds to the decay rate of the signal envelope. The subsequent analysis will show that applying $L(t')$ reveals peaks at their expected wavenumber positions in the 2D spectra. These expected positions are known exactly because, in the calculated spectra, the Hamiltonian is an input parameter. Unlike the original application of this filter in NMR, which exclusively sets t_0' =

0, we set $t_0' > 0$ to reduce the fastest-decaying components of the signal envelope, which contribute the most to spectral broadening.[27] The experimental data are initially phased as discussed in section 6 of the SI, while spectra calculated from HEOM do not require phasing. The Lorentz-Gauss filter is subsequently applied to both the coherence- and rephasing-time domains. Subsequent application of a Fourier transform with respect to the coherence and rephasing times yields the filtered 2D spectra. For further consideration of noise and vibrational mixing effects, see Sec. 8 of the SI.

HEOM treats the system-environment interactions of an individual complex explicitly using an Ohmic coupling model. The Lorentz-Gauss filter was applied to the calculated FMO spectrum. The Hamiltonian was constructed using the values from Cho et al. for BChl *a* sites I-VII,[9] plus an additional eighth site. Like the other sites, the off-diagonal elements of this eighth site were determined by modeling the dipole-dipole interactions[38] using coordinates from the X-ray structure of FMO from *C. tepidum* (PDB: 3ENI).[14] Site VIII was assigned to ω_{VIII} = 12700 cm^{-1}, and 2D spectra were calculated as described in the Methods section and Sec. 1 of the SI (Fig. 2). As t_0' increases, the individual peak frequencies become apparent at many diagonal- and cross-peak positions. We note that the calculated spectra were only intended to test outcome of the Lorentz-Gauss filtering, so a previously published Hamiltonian was used, except for the addition of site 8 as indicated.

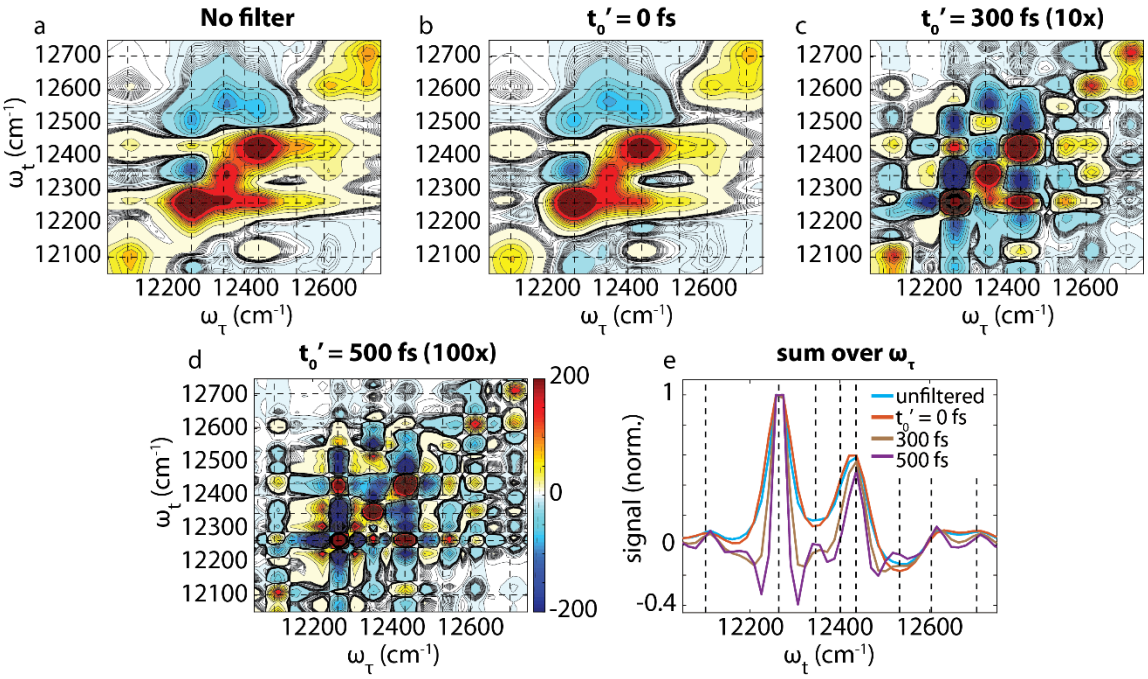

Figure 2. (a-d) 2D spectra of FMO are shown, which were calculated using HEOM. The application of the Lorentz-Gauss filter distinguishes peak positions, according to the parametrization of t_0'. The total signal diminishes as t_0' increases, so the color bar limits have been reduced by factors of 10 or 100 in panels c or d, respectively. (e) The normalized spectra are shown after summation over ω_τ. In each panel, black dotted lines represent the known exciton wavenumbers from the input Hamiltonian. They are not obtained by spectral fits. In these plots, the phased rephasing spectra are shown at T = 270 fs.

The peak positions correspond to the expected values, based on the input Hamiltonian. At t_0' = 500 fs, significant negative shoulders appear at some of the peaks, so we use t_0' = 300 fs for the subsequent analysis and expect slight negative valleys in between spectral features. For further tests of the filtering method, see Sec. 3 of the Supplemental Information.

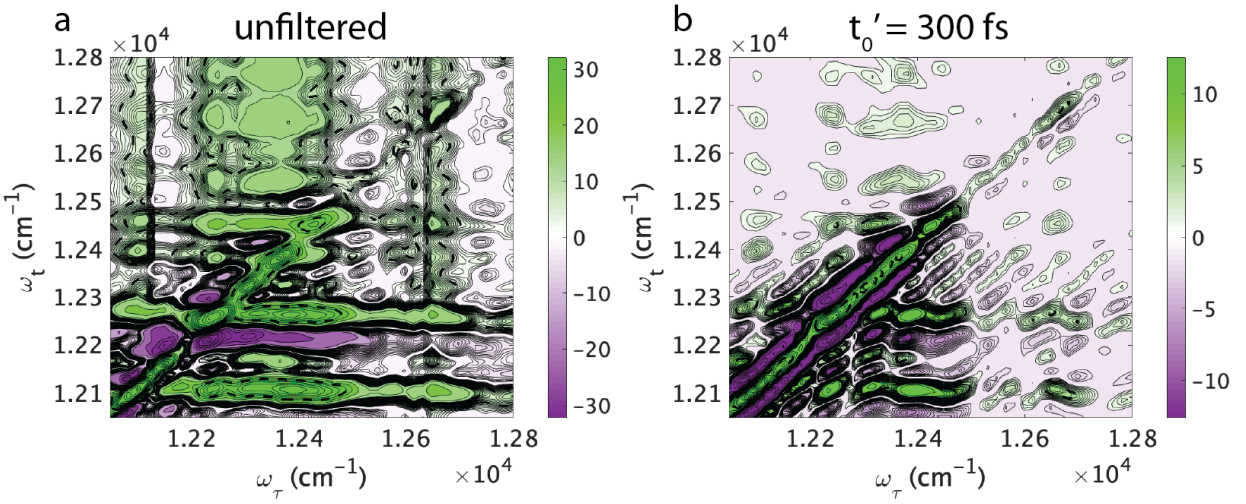

Figure 3. Measured 2D combined (rephasing and non-rephasing) spectra of FMO are shown after averaging over T to improve the signal-to-noise ratio. (A representative unaveraged spectrum is shown in Fig. S6, Supplemental Information). The "unfiltered" spectrum was obtained without the Lorentz-Gauss filter. An unusual amount of signal up to 1 ps in coherence and rephasing time were retained, in anticipation of using the LG filter. (For an example of a spectrum using smaller apodization windows, see Fig. S16 in the SI.) The other spectrum was obtained by applying the Lorentz-Gauss filter at t_0' = 300 fs. Underlying spectral peaks of the heavily overlapping regions within the spectrum can be resolved using the Lorentz-Gauss filtering method. The enhancement is evident, for example, in the area below the rephasing time of 12300 cm^{-1}. The dotted, black lines indicate cut-offs where the contour step size has been increased.

The Lorentz-Gauss filter is applied to the experimentally obtained time series at t_0' = 300 fs (Fig. 3). All else being equal, a faster decay envelope in the time-domain corresponds to broader peaks in the corresponding wavenumber domain. Many diagonal- and cross-peaks become apparent at t_0' = 300 fs. As a cautionary note, while random noise does not appreciably affect the signal in the optical spectral range (Fig. S8 in the SI), the diminished signal will still lower the S/N ratio. There are two ways that the approach used here can do so. First, because the coherence-domain range spanned picoseconds instead of a few hundred femtoseconds, it introduced more low-signal contributions at the later time

delays. As a result, the noise contribution is larger, compared to spectra obtained using a few hundred femtosecond coherence-time range. Second, the Lorentz-Gauss filter can amplify some of the region at later time delays where the signal intensity is lower (Fig. S4 in the SI), while diminishing the highest-intensity part of the signal near time zero. This effect also diminishes the signal more than the noise. As a result, the signal maxima are lowered with respect to the background.

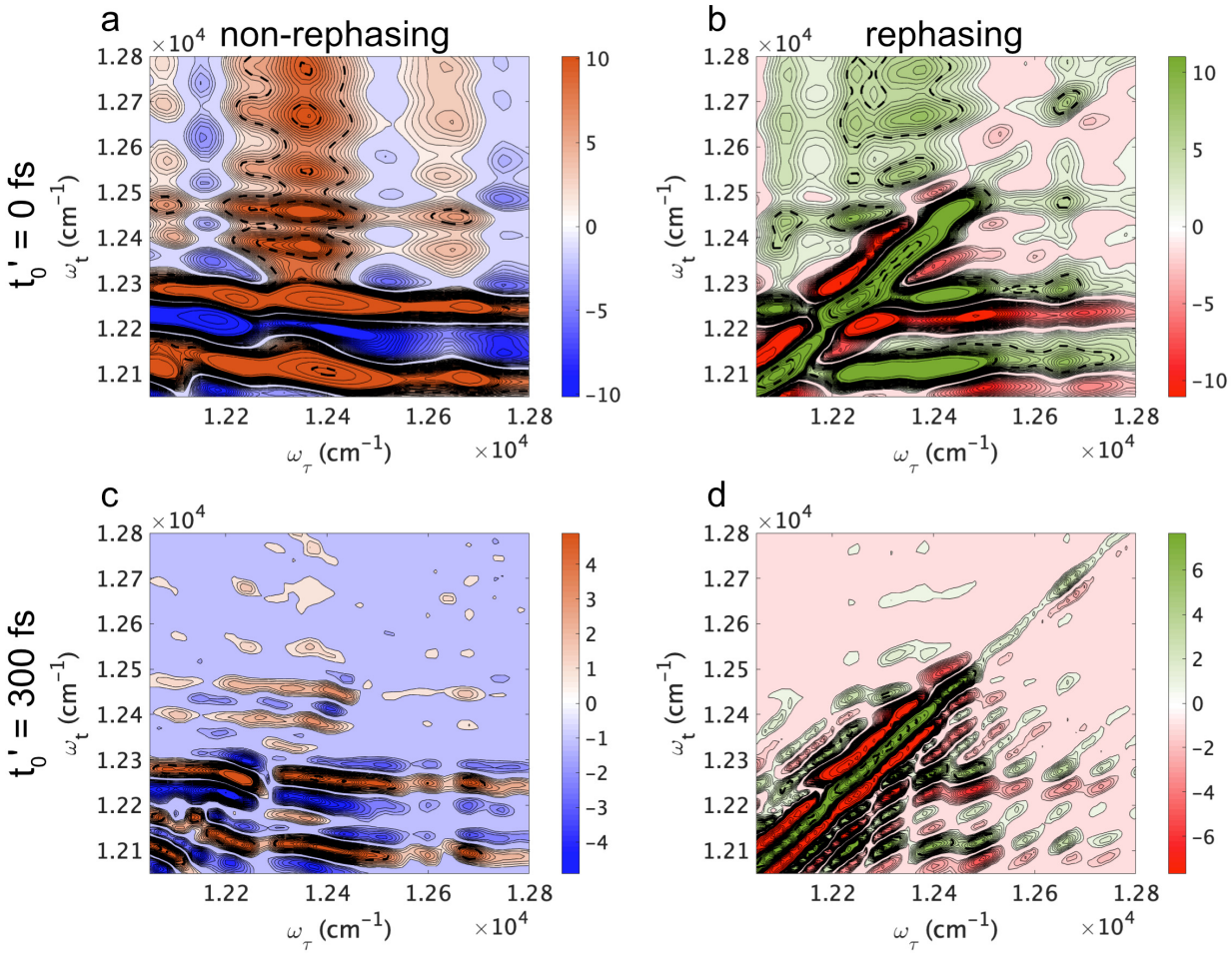

Figure 4. The rephasing and non-rephasing components of the measured 2D spectra for FMO are shown, after summation over T. The t_0' position is set to either 0 (top) or 300 fs (bottom), and the rephasing (τ > 0 fs) or non-rephasing (τ < 0 fs) components of the spectra are indicated in the figure. The more distinct peaks at larger t_0' is evident not only in the combined spectra (Figure 3), but also in the individual rephasing and non-rephasing

components of the spectra. The dotted, black lines indicate cut-offs where the contour step size has been increased, for clarity.

Figure 4 shows the individual rephasing and non-rephasing contributions to the 2D spectra. Although the rephasing and non-rephasing spectra look distinct due to their different Liouville pathways, their peak positions are both derived from the same energy levels within the chemical system, and therefore these positions should coincide.

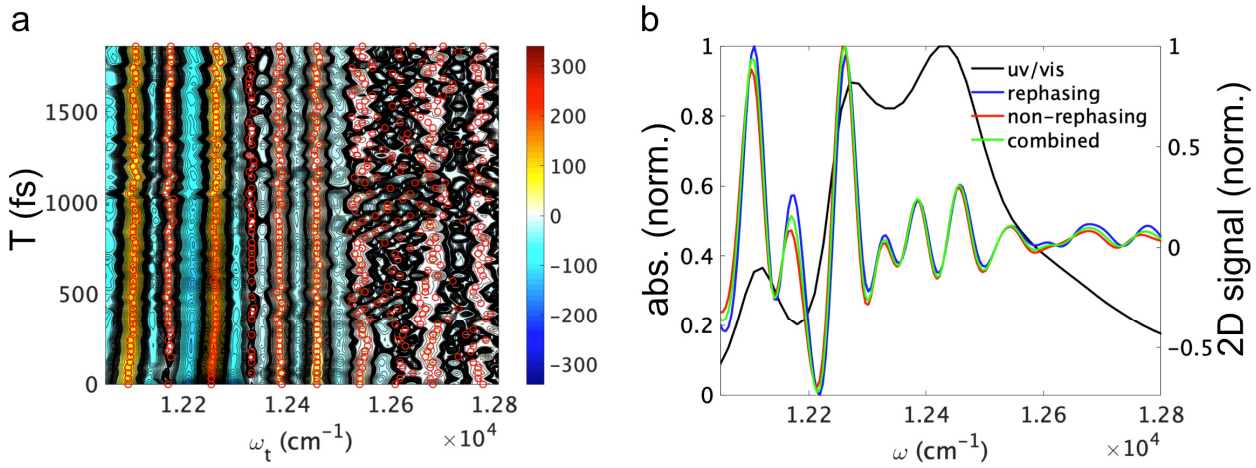

Figure 5. (a) The spectra are plotted after summation of the ω_τ axis, as a function of T. The red circles in each row indicate the peak positions located by the findpeaks algorithm in MATLAB. The average peak wavenumbers, and their standard deviations, are tabulated in Table 1 (b) The measured linear absorption spectrum (black) at 77 K is plotted along with the rephasing (blue), non-rephasing (red) and combined (green) measured 2D spectra after summation over ω_τ and T. The peak positions in the rephasing and non-rephasing spectra match, as theoretically expected, indicating that the filter acts consistently on signals generated from both sets of Liouville paths.

To compare these peak positions, first the rephasing and non-rephasing spectra are reduced to an easily comparable format by summing over ω_τ and T, yielding a data set

along ω_t (Figure 5b). The peaks' wavenumber positions obtained using this method are 12102, 12167 , 12261, 12337, 12425, 12543, 12596, 12627, and 12712 cm^{-1}. At t_0' = 300 fs, many of the peaks are distinguished in both the rephasing and non-rephasing spectra (Fig. 5).

Several of the peak assignments made here coincide with those made by previous studies (Table 1). The second peak at 12167 cm^{-1} is likely due to the second-lowest (n=1) vibrational mode of exciton 1, or a vibronic alternative. Due to the presence of this peak, which ostensibly partially overlaps with the n=0 exciton 1 signal in the uv/vis spectrum, we find an exciton 1 energy assignment of 12101 cm^{-1} that is about 10 cm^{-1} redder than the closest previous assignment made by Vulto et. al. For exciton 2, the value of 12261 cm^{-1} is exactly the same as that by Vulto et. al. The assignments for excitons 3 and 4 are within the range of those from previous studies. Exciton 5 is 42 cm^{-1} blue of the closest assignment by Schmidt am Busch et al., perhaps explained the its standard deviation of 35 cm^{-1}.

The assignment ranges are especially large at 149, 129, and 168 cm^{-1} for excitons 6-8, respectively. The disparity is likely explained by the low intensity of these peaks compared to the others, which makes it so that samples dilute enough to reduce signal reabsorption in the most intense peaks render these less intense peaks too weak to observe easily. Here, the primary interest is to measure the positions of the smaller-intensity peaks with the largest diversity of assignments, especially that for exciton 8. To obtain signal from this low-intensity region of the spectrum, it was necessary to use an increased sample concentration (Fig. S1 in the SI). Therefore, we note that the OD in the window of 12,300 – 12,500 cm^{-1}, the region with the highest extinction coefficients, was in the range of 0.3-0.4, instead of the recommended range of <0.3. This increase can lead to some

signal reabsorption and reduce their peak intensities within the nonlinear spectra. By the same token, because these peaks are so prominent, the reduced intensity does not harm the ability to determine their peak positions. Furthermore, as discussed previously, the values obtained for peaks within this wavenumber range are consistent with previous assignments (Table 1), corroborating their assignments here. Meanwhile, at this concentration, exciton 8's OD was approximately 0.05, which is near the detection limit for our spectrometer. As a result, the signal is weaker at the bluer wavenumbers, as seen in Figure 5a.

Two more issues add to the difficulty of obtaining these eigenenergies. First, the spectral overlap of these last three peaks with each other produces a featureless, smooth decline in the linear absorption spectrum from approximately 12550 – 12800 cm^{-1}, rather than the peak structures more evident from 12000 – 12550 cm^{-1}, which makes it more difficult to identify their peak positions (Figure 5b). Second, exciton 8 has fewer assignments than the other excitons, because it was first reported in 2009.[14]

At 12596 cm^{-1}, our exciton 6 assignment supports the bluer side of the range from previous assignments. Meanwhile, our assignment of 12627 cm^{-1} for exciton 7 is in the middle of the range of previous assignments, very similar to the value of 12622 cm^{-1} assigned by Cho et. al. The assignment of exciton 8 to 12712 cm^{-1} exactly matches that proposed earlier by Schmidt am Busch et al.[15] Though our exciton 8 assignment has a standard deviation of 48 cm^{-1} due to the weak intensity of the peak, this value is still smaller than the range of assignments, and our result supports the blue edge of the distribution from previous assignments.

Table 1. Exciton energies of previously published Hamiltonians are listed, as well as the one proposed here. All numbers are listed in units of wavenumbers (cm^{-1}), and the standard deviations of this work are reported, as obtained from multi-Gaussian spectral fits shown in Fig. 5a. The work by Adolphs & Renger assigned four sets of coupling constants in the site basis, using different electrostatic models. We listed the set obtained using the MEAD program. The results from the other models are available in the following reference. [10] The numbers obtained from Olbrich et al. include a 42 meV offset referenced in that work. [13] Where available, monomer Hamiltonians were used rather than trimer ones, and eight-site Hamiltonians were used rather than seven-site ones.

	Hamiltonians								
exciton	Vulto et al, 1998[39]	Cho et al, 2005[9]	Adolphs & Renger, 2006[10]	Hayes & Engel, 2011[12]	Schmidt am Busch, et al., 2011[15]	Kell et al, 2016[17]	Olbrich et al, 2016[13]	Thyrhaug et al, 2016[40]	This work
1	12112	12116	12181	12121	12171	12128	12001	12121	12102±5
2	12261	12275	12284	12274	12342	12275	12044	12275	12261±6
3	12355	12363	12358	12350	12361	12350	12079	12348	12337±4
4	12414	12405	12454	12415	12458	12391	12147	12415	12425±19
5	12448	12422	12479	12454	12501	12434	12221	12487	12543±35
6	12610	12592	12584	12520	12560	12461	12250	12581	12596±16
7	12650	12622	12679	12606	12674	12556	12291	12685	12627±8
8	-	-	-	-	12712	12615	12544	12650	12712±43

Conclusion

Weak one-quantum coherence signals were observed in FMO's 2D electronic spectra that persist at 1 ps delay. This component allows Lorentz-Gauss filtering methods[27] to be used, reducing the broadest contributions to the peak widths in the corresponding frequency-domain spectra, and therefore producing more narrow spectral features. We establish that the filtering method works correctly on these signal components in spectra calculated using HEOM. Finally, we obtain the peak positions from the narrowed 2D spectral peak structure.

Supplemental Information. Additional information is available about experimental, filtering, and analysis details; measurement reproducibility; phasing; and comparisons to previously published spectra. This material is available free of charge via the Internet at http://pubs.acs.org.

Acknowledgements

This work was supported by the Department of Defense as part of the Vannevar Bush Fellowship (N00014-16-1-2513), the Air Force Office of Scientific Research (AFOSR FA9550-14-1-0367 & FA9550-15-1-0099), and the Dreyfus Foundation. SY, SK, and GSE were supported by the Qatar National Research Foundation exceptional grant: NPRPX-107-1-027. Additional support was provided by the Chicago MRSEC, which is funded by the NSF through grant DMR-1420709. MAA acknowledges support from an Arnold O. Beckman Postdoctoral Fellowship from the Arnold and Mabel Beckman Foundation, and from a Yen Postdoctoral fellowship from the Institute for Biophysical Dynamics at The University of Chicago. RJC, KA and ATG thank the Photosynthetic Antenna Research Center (PARC), an Energy Frontier Research Center funded by the Department of Energy, Office of Science, Office of Basic Energy Sciences under Award Number DE-SC0001035 for funding. We thank Dr. Karen Watters for scientific editing.

ORCID ID

Richard J. Cogdell: 0000-0003-2119-6607

References

1. Fenna, R. E.; Matthews, B. W., Chlorophyll arrangement in a bacteriochlorophyll protein from Chlorobium limicola. *Nature* **1975,** *258*, 573-577.
2. Savikhin, S.; Buck, D. R.; Struve, W. S., Toward Level-to-Level Energy Transfers in Photosynthesis: The Fenna−Matthews−Olson Protein. *J. Phys. Chem. B* **1998,** *102* (29), 5556-5565.
3. Engel, G. S.; Calhoun, T. R.; Read, E. L.; Ahn, T.-K.; Mančal, T. s.; Cheng, Y.-C.; Blankenship, R. E.; Fleming, G. R., Evidence for wavelike energy transfer through quantum coherence in photosynthetic systems. *Nature* **2007,** *446* (7137), 782-786.
4. Cao, J.; Cogdell, R. J.; Coker, D. F.; Duan, H.-G.; Hauer, J. R.; Kleinekathöfer, U.; Jansen, T. L. C.; Mančal, T. S.; Miller, R. J. D.; Ogilvie, J. P., et al., Quantum biology revisited. *Sci. Adv.* **2020,** *6*, 1-12.
5. Pearlstein, R. M., Theory of the optical spectra of the bacteriochlorophyll a antenna protein trimer from Prosthecochloris aestuarii. *Photosynth. Res.* **1992,** *31*, 213-226.
6. Gülen, D., Interpretation of the Excited-State Structure of the Fenna-Matthews-Olson Pigment Protein Complex of Prosthecochloris aestuarii Based on the Simultaneous Simulation of the 4 K Absorption, Linear Dichroism, and Singlet-Triplet Absorption Difference Spectra: A Possible Excitonic Explanation? *J. Phys. Chem* **1996,** *100*, 17683-17689.
7. Louwe, R. J. W.; Vrieze, J.; Hoff, A. J.; Aartsma, T. J., Toward an Integral Interpretation of the Optical Steady-State Spectra of the FMO-Complex of Prosthecochloris aestuarii. 2. Exciton Simulations *J. Phys. Chem. B* **1997,** *101*, 11280-11287.
8. Vulto, S. I. E.; de Baat, M. A.; Neerken, S.; Nowak, F. R.; van Amerongen, H.; Amesz, J.; Aartsma, T. J., Excited State Dynamics in FMO Antenna Complexes from Photosynthetic Green Sulfur Bacteria: A Kinetic Model. *J. Phys. Chem. B* **1999,** *103* (38), 8153-8161.
9. Cho, M.; Vaswani, H. M.; Brixner, T.; Stenger, J.; Fleming, G. R., Exciton Analysis in 2D Electronic Spectroscopy. *J. Phys. Chem. B* **2005,** *109* (21), 10542-10556.
10. Adolphs, J.; Renger, T., How Proteins Trigger Excitation Energy Transfer in the FMO Complex of Green Sulfur Bacteria. *Biophys. J.* **2006,** *91* (8), 2778-2797.
11. Müh, F.; Madjet, M. E.-A.; Adolphs, J.; Abdurahman, A.; Rabenstein, B. r.; Ishikita, H.; Knapp, E.-W.; Renger, T., Alpha-Helices direct excitation energy flow in the Fenna–Matthews–Olson protein. *Proc. Nat. Acad. Sci. USA* **2007,** *104*, 16862-16867.
12. Hayes, D.; Engel, G. S., Extracting the Excitonic Hamiltonian of the Fenna-Matthews-Olson Complex Using Three-Dimensional Third-Order Electronic Spectroscopy. *Biophys. J.* **2011,** *100* (8), 2043-2052.
13. Olbrich, C.; Jansen, T. L. C.; Liebers, J. r.; Aghtar, M.; Strümpfer, J.; Schulten, K.; Knoester, J.; Kleinekathöfer, U., From Atomistic Modeling to Excitation Transfer and Two-Dimensional Spectra of the FMO Light-Harvesting Complex. *J. Phys. Chem. B* **2011,** *115* (26), 8609-8621.
14. Tronrud, D. E.; Wen, J.; Gay, L.; Blankenship, R. E., The structural basis for the difference in absorbance spectra for the FMO antenna protein from various green sulfur bacteria. *Photosynth. Res.* **2009,** *100* (2), 79-87.
15. Schmidt am Busch, M.; Müh, F.; El-Amine Madjet, M.; Renger, T., The Eighth Bacteriochlorophyll Completes the Excitation Energy Funnel in the FMO Protein. *J. Phys. Chem. Lett.* **2011,** *2* (2), 93-98.
16. Yeh, S.-H.; Kais, S., Simulated two-dimensional electronic spectroscopy of the eight-bacteriochlorophyll FMO complex. *J. Chem. Phys.* **2014,** *141* (23), 234105.

17. Kell, A.; Blankenship, R. E.; Jankowiak, R., Effect of Spectral Density Shapes on the Excitonic Structure and Dynamics of the Fenna–Matthews–Olson Trimer from Chlorobaculum tepidum. *J. Phys. Chem. A* **2016,** *120* (31), 6146-6154.
18. Saer, R. G.; Stadnytskyi, V.; Magdaong, N. C.; Goodson, C.; Savikhin, S.; Blankenship, R. E., Probing the excitonic landscape of the Chlorobaculum tepidum Fenna-Matthews-Olson (FMO) complex: a mutagenesis approach. *BBA - Bioenergetics* **2017,** *1858* (4), 288-296.
19. Flanagan, M. L.; Long, P. D.; Dahlberg, P. D.; Rolczynski, B. S.; Massey, S. C.; Engel, G. S., Mutations to R. sphaeroides Reaction Center Perturb Energy Levels and Vibronic Coupling but Not Observed Energy Transfer Rates. *J. Phys. Chem. A* **2016,** *120* (9), 1479-1487.
20. Milder, M. T. W.; Brüggemann, B.; Grondelle, R.; Herek, J. L., Revisiting the optical properties of the FMO protein. *Photosynthesis Research* **2010,** *104* (2-3), 257-274.
21. Scholes, G. D.; Fleming, G. R.; Chen, L. X.; Aspuru-Guzik, A.; Buchleitner, A.; Coker, D. F.; Engel, G. S.; van Grondelle, R.; Ishizaki, A.; Jonas, D. M., et al., Using coherence to enhance function in chemical and biophysical systems. *Nature* **2017,** *543* (7647), 647-656.
22. Mukamel, S., *Principles of Nonlinear Optical Spectroscopy*. Oxford University Press: New York, 1995.
23. Zheng, H.; Caram, J. R.; Dahlberg, P. D.; Rolczynski, B. S.; Viswanathan, S.; Dolzhnikov, D. S.; Khadivi, A.; Talapin, D. V.; Engel, G. S., Dispersion-free continuum two-dimensional electronic spectrometer. *Appl. Opt.* **2014,** *53* (9), 1909-1917.
24. Panitchayangkoon, G.; Hayes, D.; Fransted, K. A.; Caram, J. R.; Harel, E.; Wen, J.; Blankenship, R. E.; Engel, G. S., Long-lived quantum coherence in photosynthetic complexes at physiological temperature. *Proc. Nat. Acad. Sci. USA* **2010,** *107* (29), 12766-12770.
25. Arsenault, E. A.; Yoneda, Y.; Iwai, M.; Niyogi, K. K.; Fleming, G. R., Vibronic mixing enables ultrafast energy flow in light-harvesting complex II. *Nature Communications* **2020**, 1-8.
26. Butkus, V.; Valkunas, L.; Abramavicius, D., Vibronic phenomena and exciton–vibrational interference in two-dimensional spectra of molecular aggregates. *J. Chem. Phys.* **2014,** *140* (3), 034306.
27. Ferrige, A. G.; Lindon, J. C., Resolution Enhancement in FT NMR Through the Use of a Double Exponential Function. *J. Magn. Res.* **1978,** *31*, 337-340.
28. Tanimura, Y.; Kubo, R., Time Evolution of a Quantum System in Contact with a Nearly Gaussian-Markoffian Noise Bath. *J. Phys. Soc. of Japan* **1989,** *58*, 101-114.
29. Löhner, A.; Ashraf, K.; Cogdell, R. J.; Köhler, J., Fluorescence-excitation and Emission Spectroscopy on Single FMO Complexes. *Sci. Rep.* **2016**, 1-7.
30. Brixner, T.; Mančal, T. s.; Stiopkin, I. V.; Fleming, G. R., Phase-stabilized two-dimensional electronic spectroscopy. *J. Chem. Phys.* **2004,** *121* (9), 4221-4236.
31. Ishizaki, A.; Fleming, G. R., Unified treatment of quantum coherent and incoherent hopping dynamics in electronic energy transfer: Reduced hierarchy equation approach. *J. Chem. Phys.* **2009,** *130* (23), 234111.
32. Shi, Q.; Chen, L.; Nan, G.; Xu, R.-X.; Yan, Y., Efficient hierarchical Liouville space propagator to quantum dissipative dynamics. *J. Chem. Phys.* **2009,** *130* (8), 084105-5.
33. Hamm, P.; Zanni, M., *Concepts and Methods of 2D Infrared Spectroscopy*. Cambridge U. Press: Cambridge, 2011.
34. Albert, J.; Schubert, A.; Engel, V., Two-dimensional vibronic spectroscopy of molecular predissociation. *New J. Phys.* **2009,** *15*, 025008.
35. Keß, M.; Engel, V., Two-dimensional femtosecond optical spectroscopy of trapping dynamics in a charge-transfer process. *Chem. Phys. Lett.* **2016,** *650*, 41-46.

36. Kreisbeck, C.; Kramer, T.; Aspuru-Guzik, A., Disentangling Electronic and Vibronic Coherences in Two-Dimensional Echo Spectra. *J. Phys. Chem. B* **2013,** *117* (32), 9380-9385.
37. Rolczynski, B. S.; Zheng, H.; Singh, V. P.; Navotnaya, P.; Ginzburg, A. R.; Caram, J. R.; Ashraf, K.; Gardiner, A. T.; Yeh, S.-H.; Kais, S., et al., Correlated Protein Environments Drive Quantum Coherence Lifetimes in Photosynthetic Pigment-Protein Complexes. *Chem* **2018,** *4* (1), 138-149.
38. Strümpfer, J.; Schulten, K., The effect of correlated bath fluctuations on exciton transfer. *J. Chem. Phys.* **2011,** *134* (9), 095102-095109.
39. Vulto, S. I. E.; de Baat, M. A.; Louwe, R. J. W.; Permentier, H. P.; Neef, T.; Miller, M.; van Amerongen, H.; Aartsma, T. J., Exciton Simulations of Optical Spectra of the FMO Complex from the Green Sulfur Bacterium Chlorobium tepidumat 6 K. *J. Phys. Chem. B* **1998,** *102* (47), 9577-9582.
40. Thyrhaug, E.; Zidek, K.; Dostál, J.; Bína, D.; Zigmantas, D., Exciton Structure and Energy Transfer in the Fenna–Matthews–Olson Complex. *J. Phys. Chem. Lett.* **2016,** *7* (9), 1653-1660.

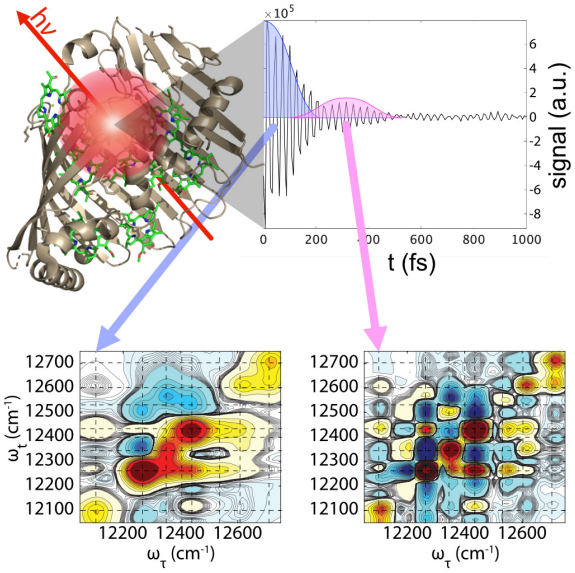
hν
×10^5
6
4
2
0
-2
-4
-6
-8
signal (a.u.)
0
200
600
800
1000
t (fs)
12700
12600
12500
12400
12300
12200
12100
ω_t (cm^-1)
12200 12400 12600
ω_τ (cm^-1)
12700
12600
12500
12400
12300
12200
12100
12200 12400 12600
ω_τ (cm^-1)

TOC figure